Ward, J. A., & Wilson, R. E. (2008). New equilibria in a multilane model of highway traffic. (pp. 20 p).

Peer reviewed version

New Equilibria in a Multilane Model of Highway Traffic

Jonathan Ward* and R. Eddie Wilson

Department of Engineering Mathematics, University of Bristol,

Queen's Building, University Walk, Bristol BS8 1TR

(Dated: January 31, 2008)

Abstract

Equilibria of a microscopic multilane traffic model are studied on a ring-road. The 'Minimising Overall Braking In Lane-changing' (MOBIL) [1] framework is coupled with an optimal velocity acceleration law that includes relative velocity (OVRV). We choose initial data that are longitudinal equilibria of the OVRV model and determine the conditions that give rise to lane-changing. We analyse the lane-changing criteria and determine a macroscopic approximation of the rate of change of density between lanes for given initial data. We observe new phenomena for unstable parameter values where the density profile in each lane synchronises and illustrate the qualitative differences when lane-changing is allowed.

PACS numbers: 05.45.-a, 45.50.-j, 47.40.-x, 47.54.-r

Keywords: Traffic modelling; Multilane; Lane-Changing; Discrete; Continuum; Microscopic; Macroscopic

*Electronic address: Jon.Ward@bristol.ac.uk

1. INTRODUCTION

Congestion problems are of great importance to economies worldwide and in the UK alone the cost has been estimated at as much as 22 billion pounds annually [2]. In the last fifteen years this has lead to a rapid growth in the study of traffic flow (see [3–5] for reviews). Recent advances in Intelligent Transport Systems (ITS) are now providing traffic scientists and engineers with the means to tackle the underlying causes of congestion. An area that will benefit from this progress is the study of multilane traffic and lane-changing. Time averaged empirical data collected from induction loops is typically too coarse to quantify the cause and effect of individual lane changes. In contrast, the emergence of Individual Vehicle Data (IVD) [6] and re-identification algorithms [6, 7] will allow lane-changing models to be refined through quantitative testing against empirical data.

In this paper we focus on the analysis of lane-changing. We simulate a microscopic multilane traffic model where the vehicles in each lane are initially in longitudinal equilibrium, but the equilibria are different in each lane. We observe two types of solution where either a finite number of lane changes occur and the system reaches a new equilibrium or no lane-changing occurs. We identify the initial conditions that give rise to lane-changing and develop a macroscopic model that approximates the discrete simulation in a well defined limit.

Macroscopic multilane models were first proposed by Gazis [8] and later Munjal and Pipes [9]. For lanes of initially constant density, $\rho_0(t)$ and $\rho_1(t)$, lane-changing was approximated in [8] by the Delay Differential Equations (DDEs)

$$\dot{\rho}_0(t) = -\dot{\rho}_1(t) = \gamma \left[\rho_1(t-\tau) - \rho_0(t-\tau) - (\rho_{10} - \rho_{00})\right], \tag{1}$$

where ρ_{00} and ρ_{10} are know equilibria and γ is a constant. In [9] a similar model without delay was used as a source term in the system of linearised hyperbolic conservation laws

$$(\rho_0)_t + c_0(\rho_0)_x = \gamma[\rho_1 - \rho_0], \tag{2}$$

$$(\rho_1)_t + c_1(\rho_1)_x = \gamma[\rho_0 - \rho_1], \tag{3}$$

to study the propagation of density perturbations introduced by an on-ramp. This was extended in [10] to account for different exchange rates in each lane. Further development of macroscopic models has been through indirect means via gas kinetic models [11, 12] and hybrid models [13].

Microscopic dynamical systems models of multilane traffic have been proposed in [14–20], where lane-changing is typically modelled with a "gap acceptance" rule. Empirical studies from in situ detectors [21] are somewhat limited because of the difficulty in obtaining large samples of suitably long trajectories with the required resolution. Vehicles with built-in monitoring systems have been used but these can be very driver specific. It is emerging from data that lane-changes are a key factor in the formation of congestion [22].

This paper is arranged as follows. In Sec. 2, we describe the microscopic model framework, specifically the detailed lane-changing criteria and longitudinal acceleration law. We then present simulation results in Sec. 3 for a particular type of initial value problem with stable parameter values and in Sec. 4 we determine which initial conditions give rise to lane-changing. We extend this in Sec. 5 to general lane-changes and link the microscopic lane-changing criteria to a macroscopic model. We then compare our numerical and analytical approximations with microscopic results. In Sec. 6, we illustrate the new phenomena that we observe when the discrete system is unstable to small perturbations. Finally in Sec. 7 we conclude and comment on our results.

2. MICROSCOPIC MULTI-LANE MODEL

We consider a large number N of identical vehicles travelling in a discrete lane $l = \{0, 1\}$ in continuous space x and time t, on a ring road of length L. Each vehicle has a position $x_n(t)$ and velocity $v_n(t)$ and travels in the increasing x direction. The subscripts $n = 1, 2, \ldots, N$ do not correlate to the order of vehicles (as in a single-lane model) since overtaking is allowed.

The variables of neighbouring vehicles (see Fig. 1) are considered when changing lanes. We restrict our attention to the four nearest neighbours: the car in front of n in the same lane n^{f}; the car behind n in the same lane n^{b}; the car in front of n in the neighbouring lane n^{fo}; and the car behind n in the neighbouring lane n^{bo}. We use the sub- and superscripts to reference variables in the same way, for example v_j^{f} refers to the velocity of the car in front of vehicle j. The distances to the neighbouring vehicles, known as headways, are measured

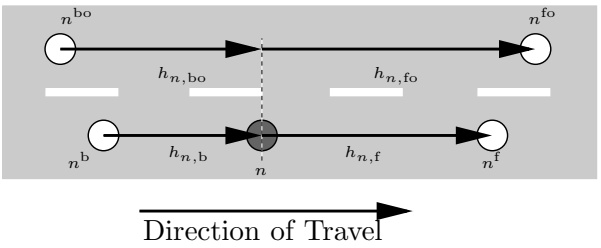

FIG. 1: Illustration of vehicles involved in a lane-change. For vehicle n (grey circle), these are labelled n^{f}, n^{b}, n^{fo} and n^{bo}. The headways, $h_{n,\mathrm{f}}$, $h_{n,\mathrm{b}}$, $h_{n,\mathrm{fo}}$ and $h_{n,\mathrm{bo}}$ respectively, are measured longitudinally and positive definite.

longitudinally,

$$h_{n,\mathrm{f}} = x_n^{\mathrm{f}} - x_n, \tag{4}$$

$$h_{n,\mathrm{b}} = x_n - x_n^{\mathrm{b}}, \tag{5}$$

$$h_{n,\mathrm{fo}} = x_n^{\mathrm{fo}} - x_n \text{ and} \tag{6}$$

$$h_{n,\mathrm{bo}} = x_n - x_n^{\mathrm{bo}}. \tag{7}$$

We apply the multi-lane model "Minimising Overall Braking in Lane-changing" (MOBIL) introduced by Kesting *et al* in [1], to the acceleration law described above. In this framework the longitudinal dynamics are not coupled to lane-changing; one is free to choose any single-lane acceleration law. The lane-changing criteria are however based on vehicle accelerations. All of the characteristics of the longitudinal model are therefore present in the lane-changing decision making process.

Under the MOBIL lane-changing rules, each vehicle calculates the difference between current acceleration, a, and the resulting acceleration if the manoeuvre is made, $\tilde{a}$, for itself and neighbouring vehicles. The criteria are split into an incentive inequality

$$\tilde{a}_n - a_n + p\left(\tilde{a}_n^{\mathrm{b}} - a_n^{\mathrm{b}} + \tilde{a}_n^{\mathrm{bo}} - a_n^{\mathrm{bo}}\right) > \tau, \tag{8}$$

and a safety inequality

$$\tilde{a}_n^{\mathrm{bo}} > -\sigma. \tag{9}$$

In Eqs. (8) and (9) p is a summation weight parameter and τ and σ are threshold parameters. The incentive criterion Eq. (8) determines the net acceleration gain (or loss) from a weighted sum (with weight p) of the difference in accelerations before and after the lane-change for

the vehicles n, n^{b} and n^{bo}. The safety criterion Eq. (9) ensures that the manoeuvre does not cause vehicle n^{bo} to brake dangerously. If the inequalities in both Eqs. (8) and (9) are satisfied then vehicle n changes lanes with probability μ in unit time.

With the weight in Eq. (8) $p > 0$, lane-changes are altruistic; the gain or loss that the trailing vehicles experience is considered when determining the incentive to change lanes. In this paper we assume lane changes to be selfish in nature and set $p = 0$.

The longitudinal acceleration law used in this paper is the Optimal Velocity (OV) model [23] with a relative velocity term, which we refer to as the OVRV model. This is given by

$$\dot{x}_n = v_n, \tag{10}$$

$$\dot{v}_n = \alpha \left\{ V(h_{n,\mathrm{f}}) - v_n \right\} + \beta \dot{h}_{n,\mathrm{f}}, \tag{11}$$

$$= a_n \left(v_n, h_{n,\mathrm{f}}, \dot{h}_{n,\mathrm{f}} \right), \tag{12}$$

where $\dot{h}_{n,\mathrm{f}} = \dot{x}^{\mathrm{f}}_n - \dot{x}_n$, α and β are parameters and V is the OV function. This function should have the properties 1. $V(0) = 0$, 2. $V' \geq 0$ and 3. $V(h) \to V_{\max}$ as $h \to 0$. It can be shown via standard techniques that the linear-stability criterion for such a model is

$$\frac{\alpha}{2} + \beta > \mathrm{maxV}'. \tag{13}$$

We will not use the exact form of the OV function in our mathematical analysis but our numerics apply the widely used S-shape

$$V(h) = \tanh(\mathrm{h} - 2) + \tanh(2). \tag{14}$$

The goal of this paper is to determine macroscopic source terms that model the lane-changing behaviour of the microscopic model described above. To achieve this, we use a particular simulation arrangement which we refer to as the Density Exchange Problem. This is a simple initial value problem in which each lane starts in longitudinal equilibrium. The headway $h_{n,\mathrm{f}}$ of each vehicle is initially the same and the velocities are given by $V(h_{n,\mathrm{f}})$. We do not however force the same equilibrium conditions in *both* lanes. We choose this type of problem because macroscopically there is no spatial variation. Microscopic quantities can then be simply averaged and compared to predictions made by macroscopic models. Our initial values are such that at time $t = 0$ there are N_0 cars in lane 0 with spacing H_0 and N_1 cars in lane 1 with spacing H_1. These values satisfy

$$N_0 H_0 = N_1 H_1 = L \qquad \text{and} \qquad N_0 + N_1 = N.$$

	Lane 0		Lane 1	
	h_0	N_0	h_1	N_1
Case a	0.75	2000	1.5	1000
Case b	1.5	1600	3.0	800
Case c	3.0	2000	12.0	500

TABLE I: Initial conditions

Vehicle velocities are chosen so that they satisfy equilibrium conditions of the longitudinal model. For the OVRV model this corresponds to $V(H_0)$ for cars in lane 0 and $V(H_1)$ for cars in lane 1.

3. MICROSCOPIC MODEL RESULTS

We solve the system of ODEs, Eqs. (10) and (11), using a standard fourth order Runge-Kutta method with a fixed time step $dt = 0.01$. The lane-changing criteria, Eqs. (8) and (9), are tested before each integration step. Values of $\alpha = 2$ and $\beta = 1.5$ are chosen such that uniform flows are linearly stable. We choose the threshold values $\tau = 0.01$, $-\sigma = -1.0$ and stochastic lane-changing rate $\mu = 0.01$; we discuss the role that these parameters play once we have presented the simulation results.

Numerical solutions of three pairs of initial headway (Table I) are illustrated in Fig. 2a-c. We refer to these as Cases a-c respectively. We calculate the mean velocity and headway in each lane and use the later to compute mean density. Two types of solution are observed for all initial values of H_0 and H_1:

Type 1. Figure 2a (heavy traffic) and c (light traffic). A finite number of lane-changes occur and the density in each lane becomes constant in time; this is not necessarily the same for both lanes.

Type 2. Figure 2b (between light and heavy traffic) No lane-changing occurs and the initial density remains constant in time.

From experiments with the initial conditions, we find that non-trivial Type 1 solutions occur in two distinct bands at high and low density. Outside of these strips only trivial Type 2 solutions exist. At high density (as in Case a), the difference in mean density between lanes

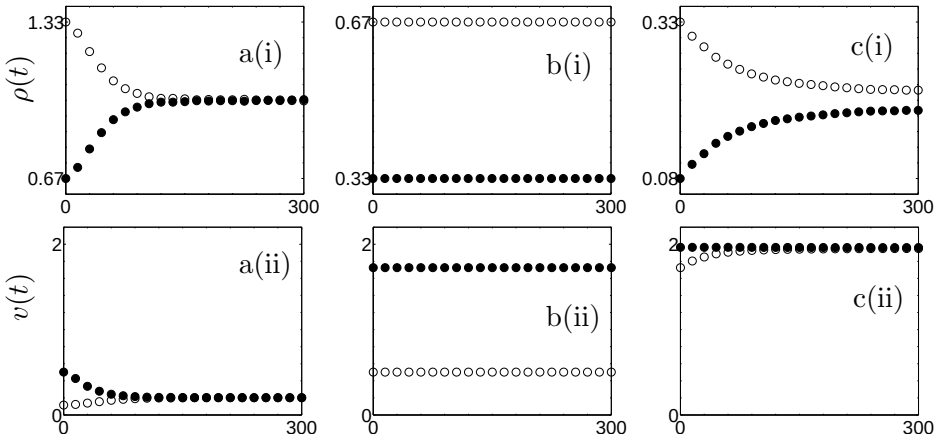

FIG. 2: Mean density (i) and velocity (ii) of lanes 0 (white markers) and 1 (black markers). For each lane, the mean density is obtained by taking the reciprocal of the arithmetic mean of the headways $h_{n,\mathrm{f}}$, and mean velocity by taking the arithmetic mean of the velocities v_n. The parameters take the following values: $\alpha = 2$, $\beta = 1.5$, $\mu = 0.001$, $\tau = 0.01$ and $-\sigma = -1.0$. There are two regions where lane changing occurs, in heavy traffic (a) and light traffic (c). There is no lane-changing for intermediate values (b).

vanishes for large time. This is not so at low density (as in Case c), where an appreciable difference remains. The velocity difference between lanes however becomes negligible.

For positive values of the threshold parameters τ and σ, we find that the solution structures of Fig. 2a-c are typical. Rather than reproduce such solution trajectories, we describe here the role that the parameters play. Decreasing the thresholds (decreasing τ and increasing σ) increases the number of initial conditions which give rise to Type 1 solutions. It also increases the rate at which the lanes reach equilibrium and decreases the equilibrium density difference between lanes. The converse is true if the threshold parameters are increased; equilibria may have appreciable velocity differences between lanes.

4. MICROSCOPIC LANE-CHANGING ANALYSIS

We would like to know *a priori* which initial conditions satisfy Eqs. (8) and (9). For the results presented in Sec. 3, we chose $H_0 < H_1$; we adopt this convention and assume that vehicles in lane 0 wish to change into lane 1. The result of choosing initial data that are equilibria of the longitudinal acceleration law Eq. (11) is that the spacing and velocity

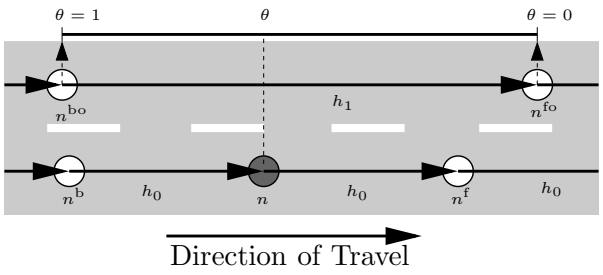

FIG. 3: The phase difference between two lanes with a constant velocity difference is described by the variable θ. For an arbitrary vehicle n in the slower of the two lanes, θ measures the vehicle's normalised position between the car in front in the other lane n^{fo} and the car behind in the other lane n^{bo}.

of vehicles remains constant until a lane-changing event. For a vehicle n (with $p = 0$) the criteria reduce to testing $\tilde{a}_n > \tau$ and $\tilde{a}_n^{\mathrm{bo}} > -\sigma$. To calculate these accelerations we need to know the velocity, headway and velocity difference of the vehicles involved. For the vehicle n changing lanes, these are $V(H_0)$ (since lane-changes are instantaneous and vehicles only accelerate once they have manoeuvred), $h_{n,\mathrm{fo}}$ and $V(H_1) - V(H_0)$ respectively, if the manoeuvre is made. Similarly, for the new follower n^{bo}, the velocity, headway and velocity difference are $V(H_1)$, $H_1 - h_{n,\mathrm{fo}}$ and $V(H_0) - V(H_1)$ respectively. The only variable left in the lane-changing criteria is $h_{n,\mathrm{fo}}$. We can simplify further by observing that the system is invariant under a shift in relative position of lanes by multiples of the distance H_1. The vehicle index can be dropped by making the substitution $h_{n,\mathrm{fo}} = \theta H_1$ and all possible values of the lane-changing criteria are accounted for in the range $\theta \in [0, 1)$. We call θ the phase difference between lanes (see Fig. 3).

For the OVRV model, the incentive and safety criteria are explicitly given by

$$\alpha \left\{V(\theta H_1) - V(H_0)\right\} + \beta \left\{V(H_1) - V(H_0)\right\} > \tau, \tag{15}$$

and

$$\alpha \left\{V((1-\theta) H_1) - V(H_1)\right\} - \beta \left\{V(H_1) - V(H_0)\right\} > -\sigma, \tag{16}$$

respectively. We plot these for Cases a-c in Fig. 4a-c respectively. The shaded regions mark where both the incentive and safety criteria are satisfied. In Case a, there is an incentive to change lanes for the entire range of θ, but it is only safe if the car makes the manoeuvre near to the leading vehicle in the other lane. Similarly in Case b, the incentive criteria are satisfied for all values of θ, but it is never safe to do so. The velocity of lanes 0 and 1 in

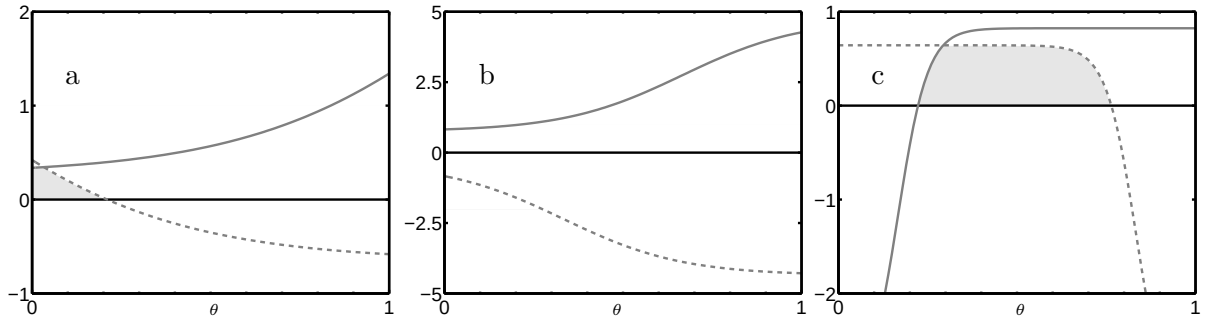

FIG. 4: The incentive (solid line) and safety (dashed line) criteria plotted against θ, the phase difference between lanes. We subtract τ from Eq. (8) and add σ to Eq. (9) so that both criteria are satisfied for values greater than zero allowing a direct comparison. Panels a-c correspond to Cases a-c. The shaded regions in a and c illustrate the values of θ where lane-changing can occur.

Case a are $V(0.75) \approx 0.11$ and $V(1.5) \approx 0.5$ respectively, whereas in Case b the velocities are $V(1.5) \approx 0.5$ and $V(3.0) \approx 1.7$ respectively. The difference in velocity between lanes is much greater in Case b, where the faster lane are travelling close to the maximum speed $V_{\max} \approx 1.96$. The criteria reflect the fact that changing lanes may be desirable but not necessarily safe. In Case c, the lane-changing criteria are satisfied in a gap between the leading and trailing vehicles in the adjacent lane.

Rather than plot Eqs. (8) and (9) for each H_0 and H_1, we will numerically calculate all of the initial conditions in (H_0, H_1)-space that satisfy both the incentive and safety criteria. Before doing this, we introduce a method of approximating general lane-changing events which naturally links microscopic and macroscopic models.

5. LANE-CHANGING AT LONGITUDINAL EQUILIBRIUM

The choice of initial conditions for our simulation greatly simplified the lane-changing criteria in Sec. 4. We now attempt to use these simplifications to study all lane-changing events by making the assumption that the acceleration of vehicles involved can be neglected before the manoeuvre. We call this the Longitudinal Equilibrium Assumption (LEA). If the lane-changing timescale is much longer than the longitudinal relaxation timescale then this assumption is valid. We can force this in our simulations by choosing small values of μ. In this section we show how we can not only estimate when the lane-changing criteria are

satisfied but we can also approximate the average rate at which vehicles change lanes and therefore directly compare solution trajectories.

For these reasons we switch to using densities rather than headways to analyse the lane-changing criteria. In longitudinal equilibrium, headway and density are simply related via $h = 1/\rho$. We use subscripts on macroscopic variables to refer to lanes and denote initial densities via $\bar{\rho}_{0,1} := 1/H_{0,1}$. We also introduce a general form of the incentive,

$$L(\theta, \rho_0, \rho_1) > 0, \tag{17}$$

and safety,

$$S(\theta, \rho_0, \rho_1) > 0, \tag{18}$$

criteria. We require that $L(\theta, \rho_0, \rho_1)$ is a strictly increasing function of θ and $S(\theta, \rho_0, \rho_1)$ is a strictly decreasing function of θ. The restrictions on the OV function in Sec. 2 mean that Eqs. (8) and (9) satisfy these requirements. For the case where lane-changes are purely selfish and $p = 0$, these conditions will be satisfied by any sensible longitudinal acceleration law. If it were not, an increase in headway would cause vehicles to decelerate.

From the above considerations we can identify two necessary conditions for lane-changing. The incentive criterion is strictly increasing in θ so it must be satisfied at $\theta = 1$,

$$L(1, \rho_0, \rho_1) > 0, \tag{19}$$

and the safety criterion is strictly decreasing in θ so it must be satisfied at $\theta = 0$,

$$S(0, \rho_0, \rho_1) > 0. \tag{20}$$

For our model, the incentive and safety criteria become

$$\hat{V}(\rho_0) = \hat{V}(\rho_1) - \frac{\tau}{\alpha + \beta}, \tag{21}$$

and

$$\hat{V}(\rho_0) = \hat{V}(\rho_1) - \frac{\sigma}{\beta} \tag{22}$$

respectively. These are found by substituting $\theta = 1$ into Eq. (8) and $\theta = 0$ into Eq. (9) and then replacing headways with densities. Similarly, we can also determine where the criteria are satisfied for all values of theta by finding $L(0, \rho_0, \rho_1) = 0$,

$$\hat{V}(\rho_0) = \frac{\beta}{\alpha + \beta}\left[\hat{V}(\rho_1) - \frac{\tau}{\beta}\right], \tag{23}$$

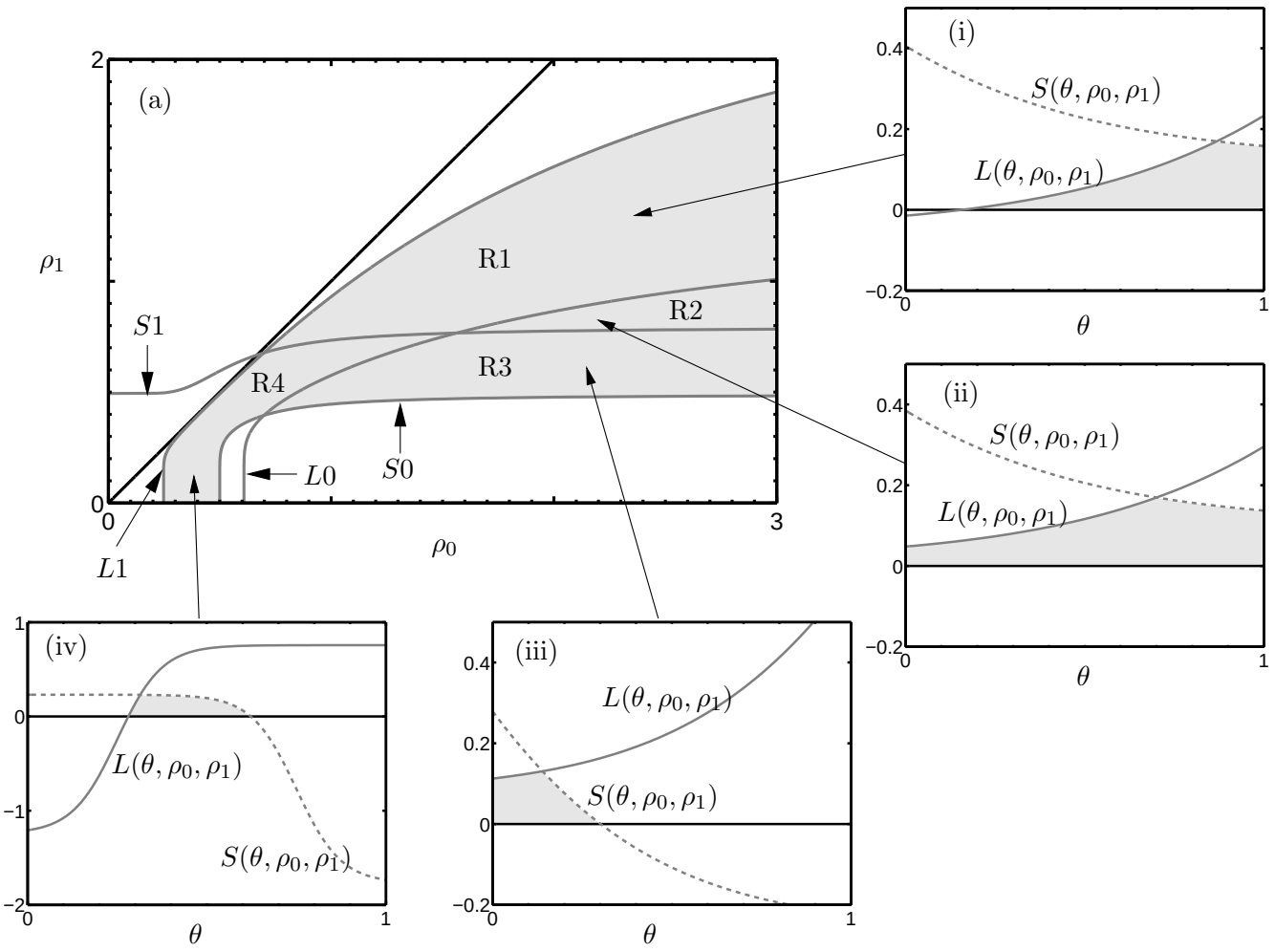

FIG. 5: Regions 1-4, labelled in (a) as R1-4 respectively, are divided by Eqs. (21)-(24), labelled $L1$, $S0$, $L0$ and $S1$ respectively. Panels (i-iv) illustrate $L(\theta, \rho_0, \rho_1)$ and $S(\theta, \rho_0, \rho_1)$ for given values of (ρ_0, ρ_1).

and $S(1, \rho_0, \rho_1) = 0$,

$$\hat{V}(\rho_0) = \frac{\alpha + \beta}{\beta} \left[\hat{V}(\rho_1) - \frac{\sigma}{\alpha + \beta} \right]. \tag{24}$$

Equations Eqs. (21) and (22) impose a condition that the model parameters must satisfy such that lane-changing can occur,

$$\sigma > \frac{\beta}{\alpha + \beta} \tau. \tag{25}$$

The curves given by Eqs. (21)-(24), split the (ρ_0, ρ_1) plane up into a maximum of four adjacent areas where the lane-changing criteria may be satisfied. These are illustrated in Fig. 5 with representative pictures of what the incentive and safety criteria may look like as a function of θ. We call these Regions 1-4 (see Table 5). For our model, the size of each

	Incentive	Safety
Region 1	$L(0, h_0, h_1) < 0$	$S(1, h_0, h_1) > 0$
Region 2	$L(0, h_0, h_1) > 0$	$S(1, h_0, h_1) > 0$
Region 3	$L(0, h_0, h_1) > 0$	$S(1, h_0, h_1) < 0$
Region 4	$L(0, h_0, h_1) < 0$	$S(1, h_0, h_1) < 0$

TABLE II: Regions in (h_0, h_1) space

Region is governed by the choice of parameters α, β, τ and σ.

For given values of ρ_0 and ρ_1 in Regions 1 and 4, monotonicity guarantees that there is a unique $\theta_L(\rho_0, \rho_1)$ that satisfies

$$L(\theta_L(\rho_0, \rho_1), \rho_0, \rho_1) = 0, \tag{26}$$

and similarly in Regions 3 and 4 there is a unique $\theta_S(\rho_0, \rho_1)$ that satisfies

$$S(\theta_S(\rho_0, \rho_1), \rho_0, \rho_1) = 0. \tag{27}$$

These values can be used to calculate the fraction of the θ-domain in which the lane-changing criteria are satisfied. We call this the Equilibrium Lane-Changing Rate (EL-CR) $\Theta(\rho_0, \rho_1)$, and compose it from each of the Regions. In Region 1

$$\Theta_{\mathrm{R1}}(\rho_0, \rho_1) = 1 - \theta_L(\rho_0, \rho_1), \tag{28}$$

in Region 2

$$\Theta_{\mathrm{R2}}(\rho_0, \rho_1) = 1, \tag{29}$$

in Region 3

$$\Theta_{\mathrm{R3}}(\rho_0, \rho_1) = \theta_S(\rho_0, \rho_1), \tag{30}$$

and finally in Region 4

$$\Theta_{\mathrm{R4}}(\rho_0, \rho_1) = \max\left(0, \theta_{\mathrm{S}}(\rho_0, \rho_1) - \theta_{\mathrm{L}}(\rho_0, \rho_1)\right). \tag{31}$$

In Fig. 6, we have used a crude numerical method to calculate $\Theta(\rho_0, \rho_1)$. For each ρ_0 and ρ_1, we divide the θ domain up into a fine grid and count the fraction of points that satisfy the lane-changing criteria. The grey-scale is used to indicate the value of $\Theta(\rho_0, \rho_1)$, the darker shades correspond to larger the values. Two distinct areas where lane-changing occurs can

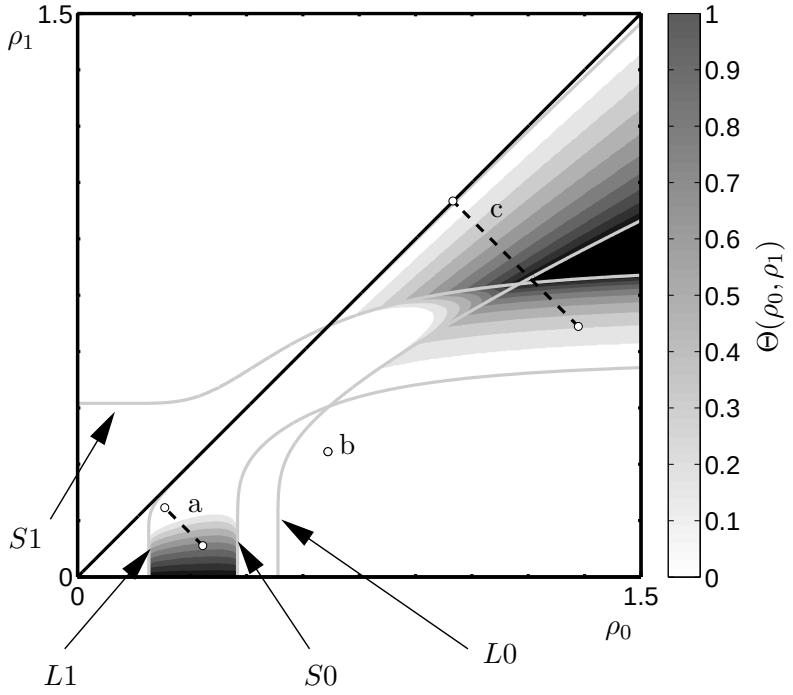

FIG. 6: Grey-scale contours of $\Theta(\rho_0, \rho_1)$ are plotted in the (ρ_0, ρ_1) plane. Overlaid on this we plot in black $\rho_0 = \rho_1$. The grey solid lines labelled L1, S0, L0 and S1 are Eqs. (21)-(24) respectively. The black dashed lines labelled a and c are solution trajectories of the microscopic simulations Cases a and c, these correspond to the solutions dipicted in Fig. 2a and c. The simulations evolve from the initial conditions (marker at the bottom right of the dashed lines) to the equilibrium solutions (marker at the top left of the dashed lines) along a straight path, each with the same gradient. The white marker labelled b is the initial conditions for Case b where lane-changing does not occur.

be seen at high and low density. These are bounded by Eqs. (21)-(24), plotted in solid grey. Solution trajectories of Cases a and c are overlaid on Fig. 6 in black dashed lines. These are straight lines because there is a direct transfer of cars (and hence density) from one lane to the other. The trajectory of Case a demonstrates that for this choice of parameters, the LEA is too restrictive and non-equilibrium events allow the density to evolve further than predicted.

We defined $\Theta(\rho_0, \rho_1)$ to be the fraction of the θ-domain over which the lane-changing criteria are satisfied. This is equivalent to the fraction of vehicles that satisfy the lane-changing criteria over some length interval. We can use this to directly approximate lane-changing macroscopically. In our model, vehicles change lanes stochastically with probability

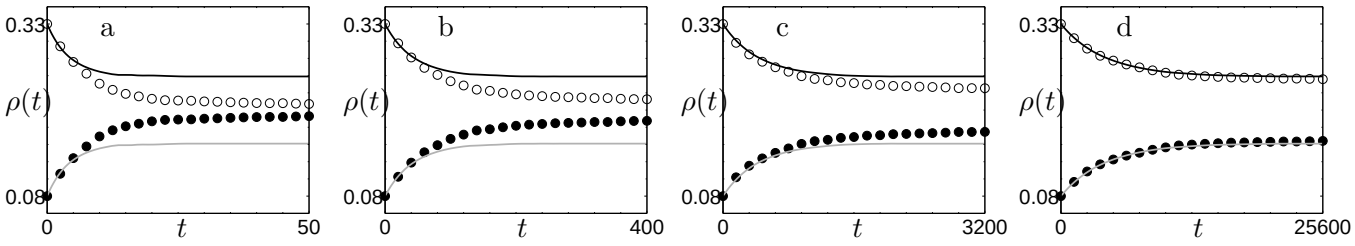

FIG. 7: Evolution of density for microscopic simulation (lane 0 - white, lane 1 - black markers) and continuum simulation (lane 0 - dash line, lane 1 - solid line) using Eqs. (34) and (35). Panels a-d correspond to Case a for the parameter values $\mu = \{0.1, 0.01, 0.001, 0.0001\}$ respectively.

$\mu\delta t$ in time δt. The density of the source lane at time $t + \delta t$ is therefore

$$\rho_0(t + \delta t) = \rho_0(t) - \Theta(\rho_0(t), \rho_1(t))\rho_0(t)\mu\delta t, \tag{32}$$

and the density of the target lane is

$$\rho_1(t + \delta t) = \rho_1(t) + \Theta(\rho_0(t), \rho_1(t))\rho_0(t)\mu\delta t. \tag{33}$$

Taking the limit $\delta t \to 0$ yields the rate of change of density flowing out of the source lane 0 and into the target lane 1

$$\dot{\rho}_0 = -\mu\Theta(\rho_0, \rho_1)\rho_0, \tag{34}$$

$$\dot{\rho}_1 = +\mu\Theta(\rho_0, \rho_1)\rho_0. \tag{35}$$

In Fig. 7a-d, we compare solutions of Eqs. (34) and (35) with microscopic simulation results for Case a using parameter values $\mu = \{0.1, 0.01, 0.001, 0.0001\}$ respectively. The macroscopic model predicts the same equilibrium densities for different lane-changing rates. In contrast the lane-changing timescale plays an important role in determining the equilibrium densities of the microscopic simulation. As the lane-changing timescale increases (as μ decreases), the LEA becomes more accurate and the agreement between the macroscopic and microscopic models improves.

Although $\Theta(\rho_0, \rho_1)$ can be calculated numerically, we have not determined its explicit form. We can however get a first order approximation in each of the Regions 1-4 if Eqs. (17) and (18) are know. To achieve this we make use of Eqs. (28)-(31) and the implicit functions $\theta_L(\rho_0, \rho_1)$ and $\theta_S(\rho_0, \rho_1)$. We Taylor expand these in ρ_0 and ρ_1 about the initial conditions

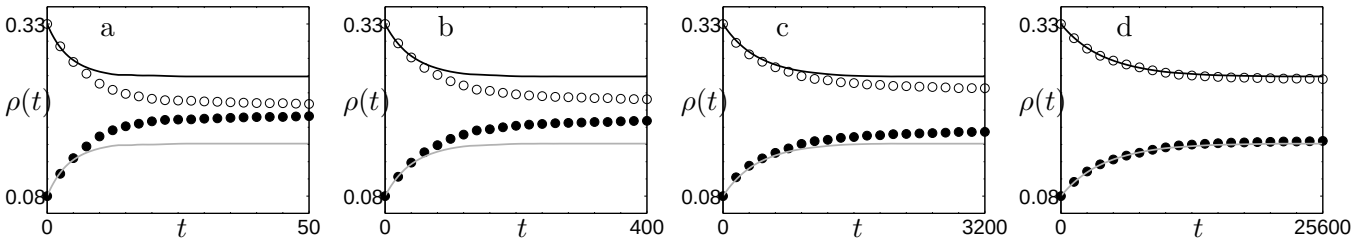

FIG. 8: Evolution of density for microscopic simulation (lane 0 - white, lane 1 - black markers) and continuum simulation (lane 0 - dash line, lane 1 - solid line) using Eqs. (38) and (39). Panels a-d correspond to Case a for the parameter values $\mu = \{0.1, 0.01, 0.001, 0.0001\}$ respectively.

$\bar{\rho}_0$ and $\bar{\rho}_1$ to first order where it is assumed that $\bar{\theta}_L := \theta_L(\bar{\rho}_0, \bar{\rho}_1)$ and $\bar{\theta}_S := \theta_S(\bar{\rho}_0, \bar{\rho}_1)$ are known. This yields

$$\theta_L(\rho_0, \rho_1) = \bar{\theta}_L + D_1\theta_L(\rho_0 - \bar{\rho}_0) + D_2\theta_L(\rho_1 - \bar{\rho}_1), \tag{36}$$

$$\theta_S(\rho_0, \rho_1) = \bar{\theta}_S + D_1\theta_S(\rho_0 - \bar{\rho}_0) + D_2\theta_S(\rho_1 - \bar{\rho}_1), \tag{37}$$

where $D_i\theta_{L,S}$ is the partial derivative of $\theta_{L,S}$ with respect to the i^{th} variable evaluated at $(\bar{\rho}_0, \bar{\rho}_1)$. We use the Implicit Function Theorem to get the partial derivatives in terms of the lane-changing criteria,

$$D_1\theta_L = \frac{D_2 L}{D_1 L}, \qquad D_2\theta_S = \frac{D_3 L}{D_1 L},$$
$$D_1\theta_L = \frac{D_2 S}{D_1 S}, \qquad D_2\theta_S = \frac{D_3 S}{D_1 S},$$

these are evaluated at $(\theta_{L,S}, \bar{\rho}_0, \bar{\rho}_1)$ respectively. For initial conditions that satisfy the lane-changing criteria in Region 4, we can write the macroscopic lane-changing model

$$\dot{\rho}_0 = -\mu\left\{\bar{\theta}_S - \bar{\theta}_L + a_0(\rho_0 - \bar{\rho}_0) + a_1(\rho_1 - \bar{\rho}_1)\right\}\rho_0, \tag{38}$$

$$\dot{\rho}_1 = +\mu\left\{\bar{\theta}_S - \bar{\theta}_L + a_0(\rho_0 - \bar{\rho}_0) + a_1(\rho_1 - \bar{\rho}_1)\right\}\rho_0. \tag{39}$$

where

$$a_0 = \left(\frac{D_2 S}{D_1 S} - \frac{D_2 L}{D_1 L}\right), \qquad a_1 = \left(\frac{D_3 S}{D_1 S} - \frac{D_3 L}{D_1 L}\right).$$

In Fig. 8a-d, we compare solutions of Eqs. (38) and (39) with microscopic simulation results (as in Fig. 7a-d) for Case a using parameter values $\mu = \{0.1, 0.01, 0.001, 0.0001\}$ respectively. The difference in equilibrium densities for Eqs. (38) and (39) is smaller than

for Eqs. (34) and (35). The solutions in Fig. 8a-d are a better approximation of the microscopic model between $\mu = 0.01$ and $\mu = 0.001$. Neither method however incorporates the dependence that the equilibrium densities have on μ.

6. LANE-CHANGING AND INSTABILITY

So far all the results presented have been in stable parameter regimes where perturbations in density are damped. In this section we illustrate some of the features that emerge when this is not the case and lane-changing is allowed. For the OVRV model, instability occurs for a range of high density values. Lane-changes perturb both the target and the source lane and these disturbances will be amplified if parameters are unstable.

Instability in macroscopic models is still a hot topic for debate and a clear approach has not yet been established. We will not therefore attempt to describe how the microscopic phenomena should be modelled at larger scales. We will continue to use macroscopic variables but we would like to illustrate the spatio-temporal growth of localised perturbations. To this end we use the coarse-graining procedure described in [24] to numerically produce densities in each lane that vary in space and time. The coarse-grained density for each individual time step is found by convolving a normalised Gaussian test function on the point distribution of vehicles, the characteristic length scale of which is large enough to smooth out individual vehicles and small enough to preserve spatial structure.

To start, we study the same model setup described in Sec. 2, where vehicles are equally spaced in each lane but the spacing differs between lanes. Numerical results are presented in Fig. 9. The first striking feature is that despite different initial conditions, the density profiles of each lane synchronise. We observe that this phenomena results from a series of catalytic events. The growth of perturbations caused by lane-changing lead to large differences in density between lanes. Vehicles moving into these congested regions respond by switching into the less dense lanes. This disturbance grows, but the densities in each lanes are now spatially correlated. Differences in density are reduced by further switching until the lanes have synchronised. As this occurs, the lane-changing rate drops and the regions with large amplitude pulses engulf the smaller ones, as in single lane models. The emergence of a single jam occurs on a much faster time scale with lane-changing. In Fig. 9 we use a relatively small number of vehicles. From experiments with larger systems, we find that there is a typical

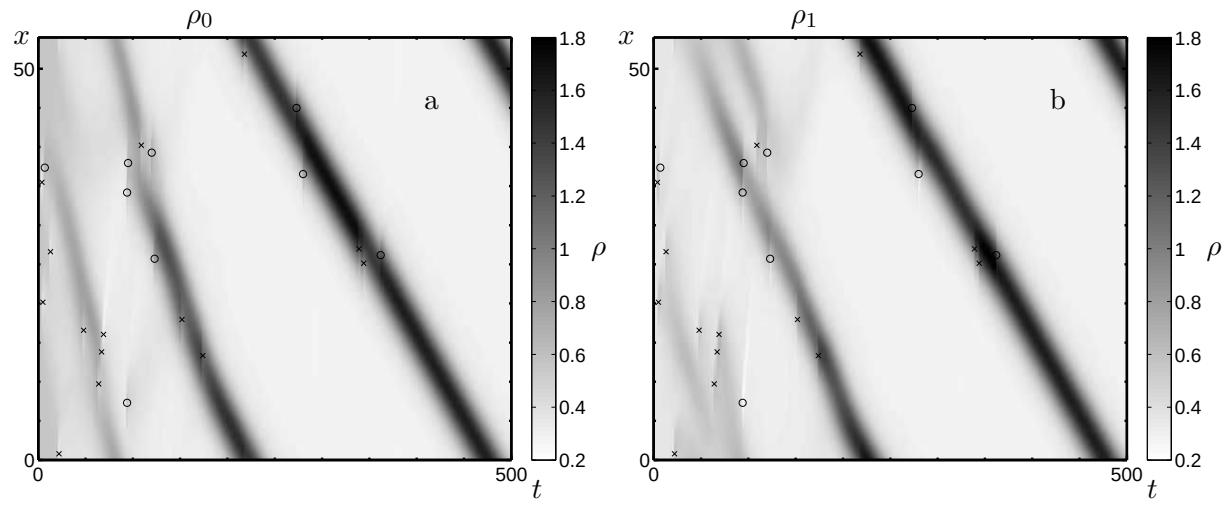

FIG. 9: Evolution of density in lane 0 (a) and lane 1 (b) from homogeneous density initial conditions as described in Sec. 2. Position on the loop x is plotted against time t and the grey-scale corresponds to coarsegrained density. Parameters are such that flows are linearly unstable, $\alpha = 0.5$, $\beta = 0.25$; the threshold parameters are $\tau = 0.01$ and $-\sigma = -2.0$; the initial conditions are $h_0 = 1.8$, $n_0 = 30$, $h_1 = 2.7$ and $n_1 = 20$ ($L = 54$). Crosses mark lane-changes from lane 0 to 1 and circles mark lane-changes from lane 1 to 0.

timescale over which the lanes synchronise and correspondingly this leads to a particular jam length scale - roughly the length of the loop in Fig. 9. Once the lanes are synchronised, lane-changing no longer occurs and the jams evolve as in a single-lane model. Over much larger time periods the jams merge until there is only one present on the loop.

Also of interest is how lane-changes affect the growth of small perturbations that are not initially caused by a lane-change. To investigate this we simulate two lanes that start from the same equilibrium condition, but perturb one vehicle in the system. This perturbation grows as in a single lane model until the difference in density between lanes causes another vehicle to switch lanes. We continue using a ring-road but choose the number of vehicles and integration time such that the leading edge of the disturbance does not interact with the trailing edge. In Fig. 10 we compare such a simulation with a similar case without lane-changing. The introduction of lane-changing in Fig. 10 a changes the characteristics of the wave profile. In particular the lane-changes at the leading edge trigger waves that do not occur in Fig. 10 b. The width of stop and go waves however does not grow in Fig. 10 a as much as Fig. 10 b.

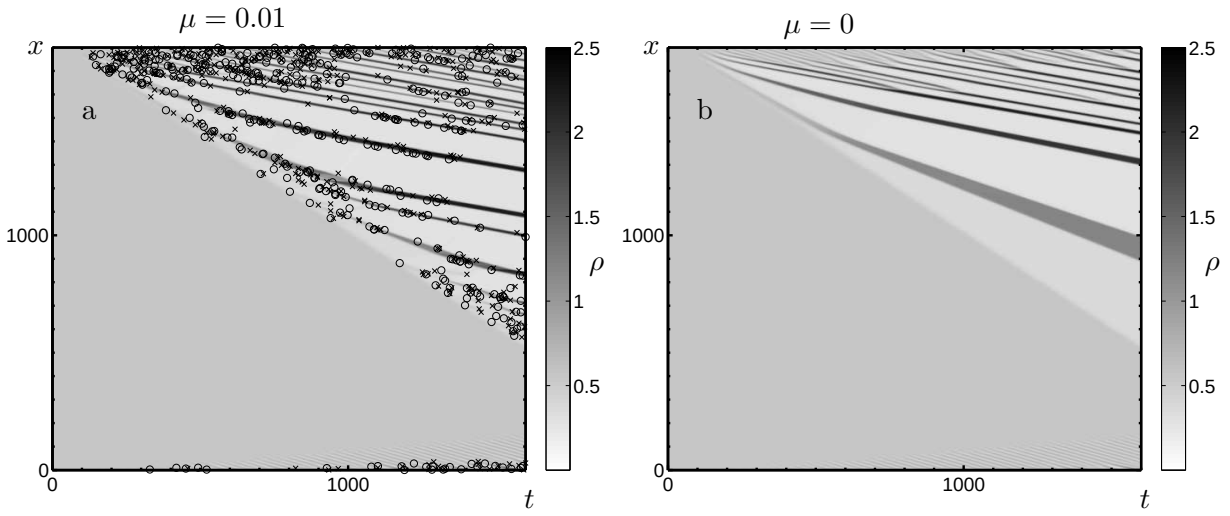

FIG. 10: Evolution of a small perturbation in density in lane 0 for unstable parameter values, $\alpha = 0.5$, $\beta = 0.25$. Lane-changing occurs in a with probability in unit time $\mu = 0.01$ but does not occur in b, where $\mu = 0$. Position on the loop x is plotted against time t and the grey-scale corresponds to coarsegrained density. Threshold parameters in a are $\tau = 0.01$ and $-\sigma = -2.0$; initial conditions are $h_0 = h_1 = 1.8$ and $n_0 = n_1 = 1000$. The perturbation is introduced by setting the velocity of one vehicle in lane 0 to $1.1V(h_0)$. Crosses mark lane-changes from lane 0 to 1 and circles mark lane-changes from lane 1 to 0. The number of steps is chosen so that the leading and trailing edges of the stop and go wave do not interact.

7. CONCLUSION

We have presented a novel analysis of lane-changing in a multilane traffic model. We have studied (what we call) the Density Exchange Problem, where vehicles in each lane are initially in equilibrium, but these equilibria are not necessarily the same in each lane. This problem has a simple macroscopic interpretation with no spatial variation and justifies averaging microscopic spacings to get macroscopic densities.

As a first step to unravelling the complex interactions that occur in such a model, we use the Longitudinal Equilibrium Assumption (LEA) to simplify the lane-changing criteria. In this simplification we assume that vehicles have negligible accelerations when changing lanes. From this we can identify the combinations of mean density in each lane that give rise to lane-changing. Furthermore, from this we find the fraction of vehicles that wish to change lanes in one direction and determine a macroscopic approximation of the microscopic

model.

In general we find that the LEA is too restrictive and the microscopic model typically reaches equilibria where the difference in density between lanes is smaller than predicted. From our analysis, we can concretely conclude that it is the *deceleration* of vehicles prior to the manoeuvre that causes this and therefore a departure from the LEA. We also observe that the microscopic equilibria depend on the stochastic parameter μ. For large values the lane-changing timescale is faster than the longitudinal relaxation timescale. The difficulty arises in the macroscopic model since our formulation fundamentally disassociates equilibria and lane-changing timescales. We cannot verify that this is a necessary feature since it could be an artifact of the microscopic simulation. It may also imply that non-local interactions are necessary in the macroscopic lane-changing law.

We have also presented some of the phenomena that we observe when the microscopic model is unstable. In particular we present the surprising result that over a short timescale the lanes synchronise. We have also illustrated how a jam develops from a small perturbation and the differences between the single and multiple lanes.

It is gradually emerging in the traffic literature, largely from empirical evidence that lane-changing is an important factor in the emergence of congestion [22]. In this paper we have analysed a particular multilane model with techniques that can be generalised to other traffic models. At present there is no standard lane-changing model and few in comparison to the number of single lane acceleration laws. Mathematical analysis of lane-changing is still in a very developmental stage.

With current ITS infrastructure increasing amounts of data are becoming available with improved resolution. In the future this may be used to unravel the key elements required by lane-changing models. We hope that this kind of data will prevent lane-changing models from falling prey to the model saturation that has occurred in the single lane case, where new models are routinely proposed, many of which fall under existing classifications.

---

[1] A. Kesting, M. Treiber, and D. Helbing, Transportation Research Record **1999**, 86 (2007).

[2] R. Eddington, *The Eddington transport study* (2006).

[3] D. Chowdhury, L. Santen, and A. Schadschneider, Physics Reports **329**, 199 (2000).

[4] B. S. Kerner, *The Physics of Traffic* (Springer-Verlag, 2004).

[5] D. Helbing, Rev. Mod. Phys. **73**, 1067 (2001).

[6] G. Lunt, R. E. Wilson, and M. Day, in *13th ITS World Congress* (2006).

[7] B. Coifman and M. Cassidy, Transportation Research Part A **36**, 899 (2002).

[8] D. C. Gazis, R. Hermann, and G. H. Weiss, Operations Research **10**, 658 (1962).

[9] P. K. Munjal and L. A. Pipes, Transportation Research **5**, 241 (1971).

[10] E. N. Holland and A. W. Woods, Transportation Research B **31**, 473 (1997).

[11] A. Klar and R. Wegener, SIAM J. Appl. Math. **59**, 983 (1999).

[12] S. P. Hoogendoorn and P. H. L. Bovy, Networks and Spatial Economics **1**, 137 (2001).

[13] J. A. Laval and C. F. Daganzo, Transportation Research Part B **40**, 251 (2006).

[14] P. G. Gipps, Transportation Research Part B **20**, 403 (1985).

[15] M. Goldbach, A. Eidmann, and A. Kittel, Phys. Rev. E **61**, 1239 (2000).

[16] D. W. Huang, Phys. Rev. E **66**, 1 (2002).

[17] S. Kurata and T. Nagatani, Physica A **318**, 537 (2003).

[18] L. C. Davis, Phys. Rev. E. **69**, 1 (2004).

[19] P. Hidas, Transportation Research Part C **13**, 37 (2005).

[20] T. Tang, H. Huang, and S. C. Wong, Acta Mech. Sin. **23**, 49 (2007).

[21] C. G. L. and K. Y. M., Transporation Research Part A **25**, 375 (1991).

[22] M. Schönhof and D. Helbing, Transporation Science **41**, 135 (2007).

[23] M. Bando, K. Hasebe, A. Nakayama, A. Shibata, and Y. Sugiyama, Phys. Rev. E **51**, 1035 (1995).

[24] H. K. Lee, H. W. Lee, and D. Kim, Phys. Rev. E **64**, 056126 (2001).